of the HO endonuclease from pGAL-HO. A brief exposure to galactose was followed by curing of pGAL-HO. Mating types were confirmed through mating and pheromone production assays. Matings produced the desired ploidy (for example, 2n *MAT***a**/**a** × 2n *MAT*α/α → 4n *MAT***a**/**a**/α/α). Ploidies of these zygotes were confirmed by tetrad dissections and analysis of mating-type segregation.

5. Total RNA was extracted and polyadenylated RNA was selected from cell samples. Using the methods of D. J. Lockhart *et al.* [*Nature Biotechnol.* **14**, 1675 (1996)] and L. Wodicka *et al.* [*ibid.* **15**, 1359 (1997)], we generated cDNA, produced biotin-labeled cRNA, hybridized fragmented cRNAs to high-density oligonucleotide arrays, stained with streptavidin-conjugated phycoerythrin, washed and scanned the arrays, and determined hybridization signal intensities, which are proportional to the target RNA concentration. Expression was measured as a trimmed average difference between 20 perfect-match and mismatch oligonucleotide probe pairs for each yeast gene. Scan-to-scan variations in intensity were corrected by a bulk scaling method analogous to adding equal amounts of total RNA to gel lanes in Northern blot expression analysis. For each scan, the sum of average differences was tallied. The median sum was found. The scaling factor for each scan (applied to each average difference in that scan) was the ratio of the median sum to the scan sum. All scaling factors were less than 2 and greater than 0.5. Scaled average differences ranged from ~0 to ~33,000; those less than 1 were set to 1.
6. All experimental cell samples were taken from asynchronous yeast cultures at late exponential phase (optical density at 600 nm = 1) growing in SC 2% glucose medium [F. Sherman, *Methods Enzymol.* **194**, 3 (1991)] at 30°C and 250 rpm. Samples were tested for viability by comparison of cell count with colony formation on plates as well as by staining with methylene blue. The growth of haploids and diploids was nearly indistinguishable. Triploids and tetraploids showed a 10 to 15% decrease in growth rates and an increased growth lag. *MAT***a**/α cells had a slight growth rate advantage and a shorter lag than their *MAT*-homozygous counterparts.
7. Expression data for each gene, as well as each reference pattern, were normalized to have mean = 0 and SD = 1. Pearson correlation coefficients were then calculated for each gene against a reference pattern either proportional to ploidy (haploids = 1, diploids = 2, and so forth) or inversely proportional (haploids = 1, diploids = 1/2, and so forth). The first criterion was that the correlation exceeded a threshold (Fig. 1). The second criterion was that the maximum and minimum average difference values for a gene differed by at least 100 units and at least a factor of 3. Ten random data sets (within-gene permutations of the experimental data set) showed that these criteria resulted in less than one false positive on average.
8. To download the data set, search the data, and view additional results, including an analysis of mating type–dependent expression, see http://staffa.wi.mit.edu/fink_public/ploidy/.
9. M. J. Kuranda and P. W. Robbins, *J. Biol. Chem.* **266**, 19758 (1991).
10. T. Galitski, A. J. Saldanha, C. A. Styles, E. S. Lander, G. R. Fink, data not shown.
11. Using the same total RNA samples used for microarray expression analysis, equal amounts of total RNA were added to each gel lane for Northern blot analysis. Radioactively probed mRNAs were visualized and quantitated by autoradiography and phosphorImager analysis. Total RNA samples derived from independent experiments (not shown) confirmed ploidy-dependent expression patterns.
12. R. K. Mortimer, *Radiat. Res.* **9**, 312 (1958); N. J. Trun and S. Gottesman, *Genes Dev.* **4**, 2036 (1990).
13. B. Futcher, *Yeast* **12**, 1635 (1996).
14. J. L. Brown *et al.*, *Genes Dev.* **11**, 2972 (1997); G. C. Chen, Y. J. Kim, C. S. Chan, *ibid.*, p. 2958.
15. T. Lechler and R. Li, *J. Cell Biol.* **138**, 95 (1997).
16. R. L. Roberts and G. R. Fink, *Genes Dev.* **8**, 2974 (1994).
17. W.-S. Lo and A. M. Dranginis, *Mol. Biol. Cell* **9**, 161 (1998).
18. ———, *J. Bacteriol.* **178**, 7144 (1996).
19. J. L. DeRisi, V. R. Iyer, P. O. Brown, *Science* **278**, 680 (1997).
20. M. Guo, D. Davis, J. A. Birchler, *Genetics* **142**, 1349 (1996).
21. B. M. Weiner and N. Kleckner, *Cell* **77**, 977 (1994); N. Kleckner and B. M. Weiner, *Cold Spring Harbor Symp. Quant. Biol.* **58**, 553 (1993).
22. B. T. Wakimoto, *Cell* **93**, 321 (1998); S. Henikoff and L. Comai, *ibid.*, p. 329.
23. Functional annotations are from the Yeast Protein Database (YPD) [P. E. Hodges *et al.*, *Nucleic Acids Res.* **27**, 69 (1999)].

24. We thank G. Acton, A. Dranginis, Q. Feng, T. Golub, M. Gordon, P. Hecht, F. Holstege, E. Jennings, F. Lewitter, H. Madhani, T. Ni, T. Orr-Weaver, J. Park, S. Rozen, D. Slonim, P. Tamayo, N. Watson, and R. Young for their contributions. Supported by Bristol-Meyers Squibb Company, Affymetrix Inc., and Millennium Pharmaceuticals Inc., and by NIH grant GM35010. G.R.F. is an American Cancer Society Professor of Genetics. T.G. is a postdoctoral fellow of the Helen Hay Whitney Foundation.

27 January 1999; accepted 13 May 1999

A Functional Assay for Centromere-Associated Sister Chromatid Cohesion

Paul C. Megee and Douglas Koshland*

Cohesion of sister chromatids occurs along the entire length of chromosomes, including the centromere where it plays essential roles in chromosome segregation. Here, minichromosomes in the budding yeast *Saccharomyces cerevisiae* are exploited to generate a functional assay for DNA sequences involved in cohesion. The centromeric DNA element CDEIII was found to be necessary but not sufficient for cohesion. This element was shown previously to be required for assembly of the kinetochore, the centromere-associated protein complex that attaches chromosomes to the spindle. These observations establish a link between centromere-proximal cohesion and kinetochore assembly.

The cohesion of replicated chromosomes (sister chromatids) is established near the time of DNA replication and persists until the metaphase-anaphase transition in mitosis. Cohesion proximal to the centromere on sister chromatids sterically constrains the centromeres so that they attach to microtubules emanating from opposite spindle poles. This ensures segregation of sister chromatids in opposition in the ensuing anaphase. In addition, the dissolution of cohesion is thought to be a key element in regulation of the metaphase-anaphase transition (*1*).

To understand the molecular basis of sister chromatid cohesion, it is necessary to identify and characterize the proteins and DNA elements important for this process. Proteins involved in cohesion have been identified and shown to be conserved from yeast to vertebrates (*2*–*4*). However, identification of requisite DNA elements has been thwarted by the fact that cohesion is not restricted to the centromere but occurs along the entire length of the chromosome (*5*, *6*). These observations suggest that cohesion factors may bind to chromosomes nonspecifically like histones or specifically to multiple sites. In either case, the DNA elements are functionally redundant, precluding their identification by classic genetic approaches.

The budding yeast is a powerful model system for analysis of DNA elements required for chromosome transmission because of the ability to construct 5- to 25-kb circular minichromosomes. Analysis of these minichromosomes led to identification of origins of replication

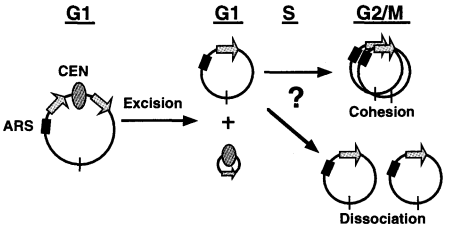

Fig. 1. Sister minichromatid cohesion assay. The minichromosome centromere (oval) is located between site-specific recombination sites (arrows). Black rectangle represents an *ARS*, the origin of replication. Hatch mark indicates the location of the test site used for mapping centromere-associated cohesion activity (see Fig. 4). Recombination results in excision of the intervening DNA, producing an acentric minichromosome and a minichromosome containing the centromere. Recombination (*8*) is induced in G_1-stage cells containing a minichromosome of interest, and cells are then released from the G_1 block. The extent of sister minichromatid cohesion on the larger, acentric minichromosomes was assessed microscopically in cells sampled after release from the G_1 block or after mitotic arrest.

Howard Hughes Medical Institute, Department of Embryology, Carnegie Institution of Washington, 115 West University Parkway, Baltimore, MD 21210, USA.

*To whom correspondence should be addressed. E-mail: koshland@mail1.ciwemb.edu

[*ARS*, ~250 base pairs (bp)] and centromere DNA (*CEN*, ~120 bp). The minichromosomes are transmitted with high fidelity, which suggests that they also contain DNA elements that mediate cohesion (*6*). However, the small size of the minichromosomes dramatically reduces the number of potentially redundant cohesion sites, facilitating the identification of cis-acting factors.

We have exploited the properties of budding yeast minichromosomes to develop an assay for cohesion sequences. We focused on the centromeric region of the minichromosome because endogenous chromosomes show cohesion proximal to the centromere, albeit at a resolution of 25 kb. A 1.6-kb DNA fragment containing centromeric DNA from chromosome III (*CEN3*) and the yeast auxotrophic marker gene *URA3* [hereafter referred to as the centromere cassette (*7*)] was placed between site-specific recombination target sites on minichromosomes. Upon recombinase induction (*8*) in G_1-stage cells, the DNA sequences flanked by recombination target sites were excised (Fig. 1). Cells were released from the G_1 cell cycle block after recombination, allowed to progress through S phase, and arrested in mitosis before the metaphase-anaphase transition. After cell fixation, minichromosome cohesion was assessed by fluorescence in situ hybridization (FISH) (*6*) or by green fluorescent protein (GFP) tags (*3, 9*). A single FISH or GFP signal is observed in G_1-stage cells containing unreplicated chromosomes or in M-stage cells in which replicated sister minichromatids are so closely associated that signals from individual sisters cannot be resolved (*8*). In contrast, two signals are observed in cells with precociously separated sister chromatids (*2, 3*). The maximal observable dissociation of sister minichromatids due to experimental limitations was 39% by GFP and about 60% by FISH (*10*).

After centromere cassette excision, the percentage of sister minichromatid dissociation was five times higher in both the FISH and GFP assays. Furthermore, the absolute amount of dissociation was about 50% of the maximum detectable levels (Fig. 2). Sister minichromatid dissociation was due to the loss of the centromere cassette rather than recombination per se because control minichromosomes that underwent centromere cassette inversion remained associated (Fig. 2A). Similar amounts of sister minichromatid dissociation were observed when the centromere cassette was excised from minichromosomes of 5 to 25 kb (Fig. 2) (*11*), which indicates that the centromere-associated cohesion function is independent of minichromosome size and sequence context. We conclude, therefore, that the centromere cassette contains DNA elements that mediate sister minichromatid cohesion.

We next examined the kinetics of the sister minichromatid dissociation. G_1-stage cells containing GFP-tagged minichromosomes were released from a G_1 block and were sampled at regular intervals for (i) minichromosome cohesion, and (ii) DNA content and endogenous chromosome dissociation to position cells within the cell division cycle (Fig. 3). Minichromatids lacking the centromere cassette began dissociating 15 min before the completion of bulk DNA replication (Fig. 3) and 15 to 30 min before the separation of endogenous sister chromatids (Fig. 3) and centromeric minichromatids (*11*). The timing of the precocious dissociation of minichromatids lacking the centromere cassette is similar to that observed for endogenous chromatids in a mutant strain defective for the cohesion protein Mcd1p/Scc1p (*3*). Thus, minichromatids lacking the cassette often begin dissociating during S phase and before the onset of anaphase, con-

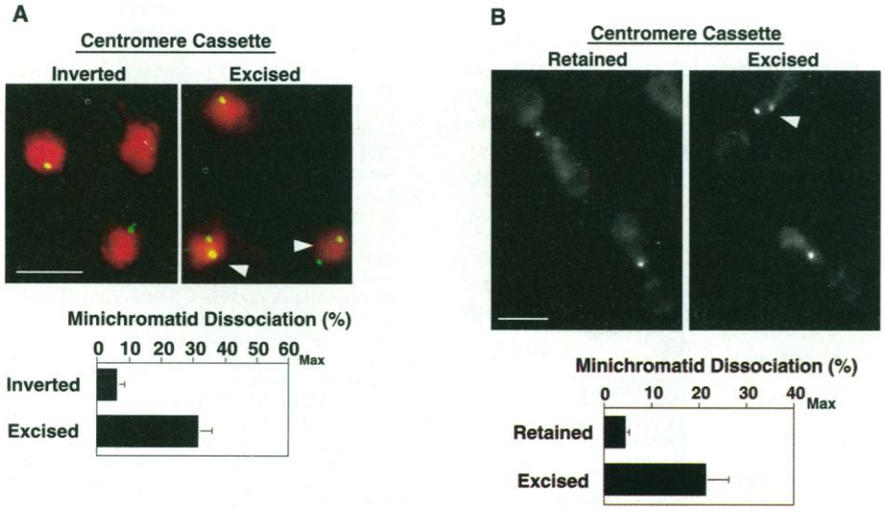

Fig. 2. Centromere cassette excision promotes sister minichromatid dissociation. Cells containing minichromosomes were released from G_1 after recombination and rearrested in mitosis by using nocodazole. (**A**) FISH analysis of nuclei containing sister minichromatids in which the centromere cassette was inverted or excised depending on the orientation of the recombination target sites. We used digoxigenin-labeled pBR322 DNA as probe to detect minichromosomes (*2, 6*), shown in green or yellow. Total chromosomal DNA, counterstained with propidium iodide, is shown in red. Sister minichromatid dissociation is plotted for three independent experiments in which FISH signals in 150 to 200 nuclei were scored. We calculated sister minichromatid dissociation by subtracting the percentage of nuclei with two FISH signals in G_1-arrested populations (representing either background hybridization or cells containing two copies of the minichromosome at the beginning of the experiment) from the percentage of nuclei with two signals after mitotic arrest. (**B**) Fixed cells containing GFP-tagged sister minichromatids (*7*) with the centromere cassette excised (recombinase induction) or retained (no recombinase induction). Sister minichromatid dissociation is plotted for six independent experiments in which GFP signals in 150 to 200 cells were scored. Max indicates maximum detectable sister minichromatid dissociation (*10*). Error bars indicate standard deviation. Bars = 5 μm. Arrowheads indicate nuclei or cells with dissociated sister minichromatids.

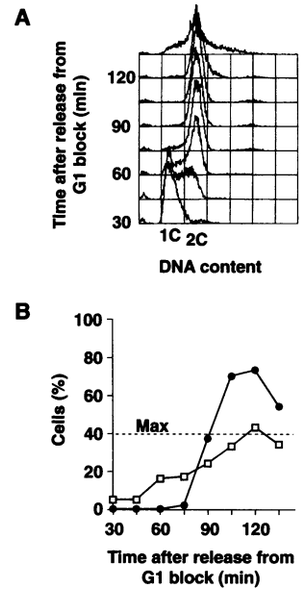

Fig. 3. Sister minichromatids lacking the centromere cassette initiate dissociation before the metaphase-anaphase transition. Cells containing GFP-tagged minichromosomes were released from a G_1 block and sampled at 15-min intervals beginning 30 min after release. (**A**) DNA content was measured by flow cytometry; 1C and 2C indicate pre- and postreplication DNA content, respectively. (**B**) Graph shows percentage of cells with dissociated sister minichromatids (squares) and dissociated endogenous sister chromatids (circles). Endogenous sister chromatid dissociation was scored in cells stained with 4′,6-diamidino-2-phenylindole. After anaphase onset, the different apparent rates of dissolution of minichromatid and endogenous chromatid cohesion probably reflects the fact that, once cohesion is eliminated, the acentric minichromatids separate only by diffusion, whereas the endogenous chromatids are actively separated by kinetochore-microtubule forces.

sistent with a failure to establish cohesion, as expected if the cassette contained a DNA element mediating cohesion.

A similar premature dissociation of minichromatids lacking the cassette was observed in time course experiments when cells were released from G_1 and blocked in metaphase by the addition of nocodazole (*11*). However, dissociation of these minichromatids reached a plateau at a value of only 50% of the maximum in metaphase-blocked cells compared with 100% of the maximum in cells that underwent anaphase. Thus the residual cohesion of the minichromatids lacking the cassette is dissolved only when the cells progress through the metaphase-anaphase transition. Because this residual cohesion exhibits the same regulation as the cohesion between endogenous chromatids, it is likely to be relevant. These data indicate that the minichromosome contains another DNA element outside the cassette that mediates cohesion.

To map the sequences within the 1.6-kb centromere cassette that are responsible for cohesion, we constructed a minichromosome in which only a 320-bp *CEN3* proximal region was excised by recombination. Removal of this sequence increased sister minichromatid dissociation fourfold (Fig. 4). We then placed a 250-bp fragment containing centromere sequences from chromosome VI (*CEN6*) between recombination target sites on another minichromosome. The only sequence similarity shared by the *CEN3* and *CEN6* fragments is the 125-bp centromere DNA. Sister minichromatid dissociation increased sevenfold when the *CEN6* sequences were removed (Fig. 4B), suggesting that the cis cohesion factor is associated with the 125-bp centromere DNA found on all yeast chromosomes.

The centromere DNA of *Saccharomyces cerevisiae* consists of three conserved centromere DNA elements (CDEs) (*12, 13*). The central element (CDEII) is ~80 bp of ≥90% A+T DNA and is flanked by two highly conserved palindromic motifs, CDEI and CDEIII. At least part of CDEII and CDEIII is required for mitotic chromosome segregation, and CDEIII is essential for assembly of the kinetochore (*14–16*). To examine the ability of these DNA elements to confer sister minichromatid cohesion activity, we placed them on the minichromosome at a test location outside the recombination target sites (Fig. 1). The centromere cassette was excised by recombination, and the remaining minichromosome containing the CDEs was then assessed for sister minichromatid dissociation. Sister minichromatids containing wild-type CDEI+II and a single base pair substitution in CDEIII (*cen3*-BCT2) showed three to four times more dissociation than minichromatids that retained the centromere cassette (Fig. 4), indicating that CDEIII is necessary for cohesion. However, minichromatids containing only CDEIII dissociated at levels similar to acentric minichromatids (Fig. 4A), indicating that CDEIII is necessary but not sufficient for cohesion activity. Thus CDEIII and its associated factors direct not only kinetochore assembly but also centromere-proximal cohesion.

In summary, our observation that cohesion at the centromere is disrupted by the removal of specific sequences suggests that cohesion proteins are not randomly distributed on chromosomes like nucleosomes but rather are positioned either by their ability to bind DNA directly or indirectly through other sequence-specific factors. Centromere-associated cohesion is thought to be critical for proper kinetochore function, and cytology of prometaphase chromosomes in other eukaryotes suggests that centromere-associated cohesion and kinetochore function are mediated by distinct complexes that lie immediately adjacent to each other. Our results suggest that, at least in budding yeast, cohesion and kinetochore activities are coordinated through a common sequence element. In principle, the minichromosome assay could also be used to define centromere-independent DNA elements mediating cohesion either by analysis of the residual cohesion of acentric minichromatids or by identification of DNA fragments that restore cohesion to acentric minichromatids.

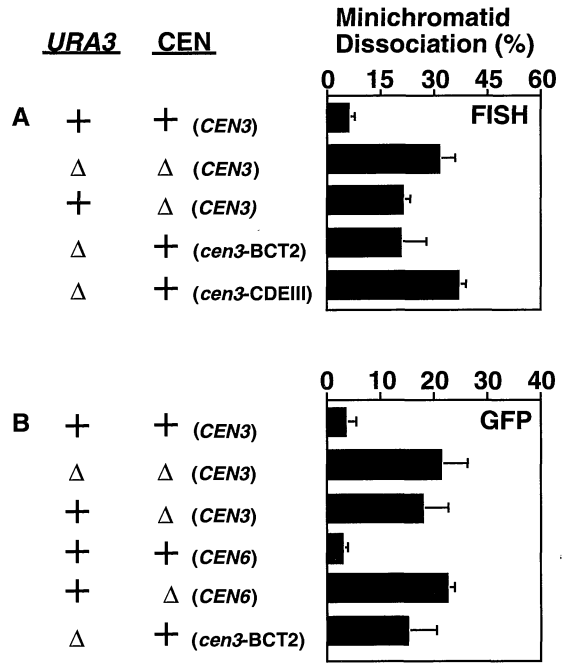

Fig. 4. Cohesion activity maps to centromeric DNA. Sister minichromatid dissociation was determined by FISH (**A**) and GFP-tagged minichromosomes (**B**). Minichromatids harboring derivatives of the original centromere cassette (*CEN3-URA3*) (*7*) or *CEN6* were tested for cohesion activity. Deletions (Δ) or substitutions (+) of centromere DNA derivatives and *URA3* are indicated. Wild-type centromeres (capital letters) and mutant *cen3* alleles are described in the text. The extent of minichromatid dissociation with or without the original centromere cassette is included for comparison (see Fig. 2). Minichromatid dissociation is plotted relative to the maximum detectable level of dissociation (*10*).

References and Notes

1. R. B. Nicklas, *Science* **275**, 632 (1997).
2. V. Guacci, D. Koshland, A. Strunnikov, *Cell* **91**, 47 (1997).
3. C. Michaelis, R. Ciosk, K. Nasmyth, *Cell* **91**, 35 (1997).
4. A. Losada, M. Hirano, T. Hirano, *Genes Dev.* **12**, 1986 (1998); R. V. Skibbens *et al.*, *ibid.* **13**, 307 (1999); A. Toth *et al.*, *ibid.* p. 320.
5. A. T. Sumner, *Chromosoma* **100**, 410 (1991).
6. V. Guacci, E. Hogan, D. Koshland, *J. Cell Biol.* **125**, 517 (1994).
7. Centromere cassettes contained a 0.3-kb Bam HI *CEN3* fragment [D. Koshland *et al.*, *Cell* **48**, 801 (1987)] and a 1.1-kb Hind III fragment encoding *URA3,* flanked by R recombinase target sites [H. Araki *et al.*, *J. Mol. Biol.* **225**, 25 (1992)]. Centromere cassettes were subcloned into the Bam HI site of pDK222 [D. Koshland, J. C. Kent, L. H. Hartwell, *Cell* **40,** 393 (1985)]. For GFP-tagged minichromosomes, an 11-kb tetracycline operator (tetO) DNA fragment encoding 224 tet repressor–GFP fusion protein (tetR-GFP) binding sites (*3*) was subcloned into the Xho I site in pDK222-based vectors.
8. Recombination is mediated by the site-specific, galactose-inducible *Zygosaccharomyces rouxii* R recombinase isolated from pHM153 [H. Matsuzaki *et al.*, *J. Bacteriol.* **172**, 610 (1990)] and integrated in two copies at *LEU2* in 1801-5A or *HIS3* in 1811-11C. Recombination was efficient: >90% of the minichromosomes had undergone recombination after 2 hours of cell growth in galactose (final concentration 2%). Yeast host strain 1801-5A was used in FISH experiments: *MAT***a** *ura3-52 his3*Δ *reg1-501 bar1 gal1*. Host strain 1811-11C was used in GFP experiments: *MAT***a** *ura3-52 bar1 can1-100 LEU2*::tetR-GFP.
9. A. Straight *et al.*, *Curr. Biol.* **6**, 1599 (1996).
10. The monitoring of sister minichromatid dissociation is limited by the ability to detect multiple FISH or GFP signals within a nucleus. The maximum dissociation of sister minichromatids occurs after the metaphase-anaphase transition when cohesion factors are inactivated. In cells with acentric sister minichromatids the number with two GFP signals after the metaphase-anaphase transition is only ~40% (see Fig. 3). This deviation from 100% reflects mostly nonphysiological associations between tetO regions and tetR-GFP on sister minichromatids. For centric minichromatids and endogenous chromatids containing tetO regions this nonphysiological association is overcome by forces mediated by the centromere and spindle microtubules. For FISH, 75% of diploid cells exhibit two FISH signals when probed with unique DNA fragments (*6*). The maximal multiple FISH signal detection limit of 75% was used, along with the percentage of centromere cassette excision (95%) and the percentage of cells that released from the G_1 block (85%), to calculate the expected sister dissoci-

ation for FISH as 60% (0.75 × 0.95 × 0.85). The validity of this estimation was demonstrated when the same calculation was applied to GFP experiments. The maximum detection of acentric minichromatid dissociation was estimated as 39%, a value very similar to the actual measured value.
11. P. Megee and D. Koshland, unpublished observation.
12. J. H. Hegemann and U. N. Fleig, *Bioessays* **15**, 451 (1993).
13. A. A. Hyman and P. K. Sorger, *Annu. Rev. Cell Dev. Biol.* **11**, 471 (1995).
14. M. Saunders, M. Fitzgerald-Hayes, K. Bloom, *Proc. Natl. Acad. Sci. U.S.A.* **85**, 175 (1988).
15. P. B. Meluh and D. Koshland, *Genes Dev.* **11**, 3401 (1997).
16. P. K. Sorger *et al.*, *Proc. Natl. Acad. Sci. U.S.A.* **92**, 12026 (1995).
17. Supported in part by NIH grant GM41718. We thank M. K. Raghuraman and R. Ciosk for plasmids and C.-M. Fan, V. Guacci, P. Meluh, and members of the Koshland Laboratory for valuable comments on the manuscript. P.C.M. was the recipient of a Cancer Research Fund of the Damon Runyon–Walter Winchell Foundation Fellowship DRG-1335.

1 April 1999; accepted 1 June 1999

Reach Plans in Eye-Centered Coordinates

Aaron P. Batista,* Christopher A. Buneo, Lawrence H. Snyder,† Richard A. Andersen‡

The neural events associated with visually guided reaching begin with an image on the retina and end with impulses to the muscles. In between, a reaching plan is formed. This plan could be in the coordinates of the arm, specifying the direction and amplitude of the movement, or it could be in the coordinates of the eye because visual information is initially gathered in this reference frame. In a reach-planning area of the posterior parietal cortex, neural activity was found to be more consistent with an eye-centered than an arm-centered coding of reach targets. Coding of arm movements in an eye-centered reference frame is advantageous because obstacles that affect planning as well as errors in reaching are registered in this reference frame. Also, eye movements are planned in eye coordinates, and the use of similar coordinates for reaching may facilitate hand-eye coordination.

To reach toward an object, information about its location must first be obtained from the retinal image. Early visual cortical areas contain topographic maps of the retina, and as a result the target is originally represented in eye-centered coordinates. However, targets for reaches should ultimately be represented in limb coordinates that specify the direction and amplitude the limb must move (motor error vector) to obtain its goal. Thus, for the brain to specify an appropriate reach command, coordinate transformations must take place. Transformation of signals from eye to limb coordinates requires information about eye, head, and limb position. These signals could be combined all at once to accomplish this transformation or in serial order to form intermediate representations in head-centered coordinates (by adding eye position information) and body-centered coordinates (by adding eye and head position information) (*1*). At some point in this process a plan to make the movement is formed; knowing how reach plans are represented in the brain can tell us much about the mechanisms and strategies the brain uses to generate reaches.

The major anatomical pathway for visually guided reaching begins in the visual cortex and passes through the posterior parietal cortex (PPC) to the frontal lobe. Different regions of PPC have recently been shown to be specialized for planning different types of movements (*2, 3*), including areas specialized for saccadic eye movements [the lateral intraparietal area (LIP)], for reaches [the parietal reach region (PRR)], and for grasping (the anterior intraparietal area). In other words, at this level of the visual-motor pathway the pattern of neural activity reflects the outcome of a movement selection process. Because PPC is partitioned into planning regions for different actions, it has been proposed that each subdivision should code its respective movement in the coordinate frame appropriate for making the movement (*4*). This proposal predicts that targets for reaches should be coded in limb coordinates in PRR. Here we demonstrate that the responses of reach-specific neurons in PRR are more consistent when reach targets are described in eye coordinates than in arm coordinates, showing that, at least in PRR, early reach plans are coded in terms of visual space rather than in terms of the limb.

Single cell recordings were made in PRR (*5*). We tested neurons in four conditions; in two conditions different reaches were performed to targets at the same retinal location, and in the other two conditions identical reaches were made to targets at different retinal locations (*6*). This paradigm allowed us to observe independently the effects on PRR neurons of manipulating target location in eye and limb reference frames. A reach-specific neuron tested in these four conditions is shown in Fig. 1. The effect of varying the initial hand position is shown in Fig. 1, A and B; the cell's spatial tuning is similar in the two conditions, showing that the cell is largely insensitive to changes in the limb-centered positions of the targets. The effect of changing the direction of gaze is shown in Fig. 1, C and D. The cell's spatial tuning changes markedly between these two conditions, even though the arm-centered locations of the targets do not change. In all conditions, the cell's preferred reach end point is constant relative to the direction of gaze—down with respect to fixation. This neuron is selectively active for reaches and encodes target location in an eye-centered reference frame.

This neuron exemplified the population of 74 neurons from three monkeys tested in this experiment. The data from all neurons are summarized by correlation analysis in Fig. 2A (*7*). Each point represents one neuron; a point's position along the horizontal axis represents the correlation between the cell's two tuning curves measured with targets at the same retinal location (conditions shown in Fig. 1, A and B). The position along the vertical axis represents the correlation between that neuron's tuning curves measured with targets at the same limb-centered location (conditions shown in Fig. 1, C and D). Eighty-four percent of the neurons lie below the line of equal correlation (*8*), showing a better correlation in an eye-centered reference frame than in a limb-centered reference frame. A second test was used in which the two tuning curves measured with the same initial hand position but with different eye positions were shifted into alignment in eye-centered coordinates (Fig. 2B). With this analysis, 81% of neurons had a correlation that was greater when the tuning curves were shifted into eye-centered alignment than when they were not shifted. Thus, the responses of most PRR neurons were better correlated for identical reach targets in eye coordinates than for identical reach targets in arm coordinates. For most neurons, spatial tuning was also more consistent in eye coordinates than in head- or body-centered coordinates; although target locations in the latter two reference frames were invariant across the four task conditions, neural responses varied with

Division of Biology and the Computation and Neural Systems Program, California Institute of Technology, Mail Code 216-76, Pasadena, CA 91125, USA.

*Present address: Howard Hughes Medical Institute and Department of Neurobiology, Stanford University School of Medicine, Fairchild Building, Room D209, Stanford, CA 94305, USA.

†Present address: Washington University School of Medicine, Department of Anatomy and Neurobiology, Box 8108, 660 South Euclid Avenue, St. Louis, MO 63110, USA.

‡To whom correspondence should be addressed. E-mail: andersen@vis.caltech.edu